United States
Department of Agriculture
Forest Service—Engineering

Remote Sensing
Applications Center

May 2004
RSAC-0068-RPT1

Postfire Burn-Severity Classification of the Hayman Fire, CO: Based on Hyperspectral Data—JFSP RFP 2001-2 Task 1

Denise Laes, Paul Maus
Remote Sensing Applications Center
USDA Forest Service
Salt Lake City, UT

Sarah Lewis, Pete Robichaud
Rocky Mountain Research Station
USDA Forest Service
Moscow, ID

Ray Kokaly
Denver Spectroscopy Lab
United States Geological Survey
Lakewood, CO

For additional information, contact Henry Lachowski, Remote Sensing Applications Center, 2222 West 2300 South, Salt Lake City, UT 84119; phone: 801-975-3750; e-mail: hlachowski@fs.fed.us.
This publication can be downloaded from the RSAC Web site: http://fsweb.rsac.fs.fed.us

Table of Contents

Abstract ..... *iv*

Introduction 1

Objectives 1

Study Area 2

Data 2

- Imagery Data 2
- Field Data: Field Spectrometer Data 3
- Field Data: Field Measurements 4
- Sampling Scheme 4
- Burn-Severity Assessment 5
- Water-Repellency Tests 5

Atmospheric Correction Methods 6

Data Analysis 8

- SWIR-BR Band Ratio Generated from ATREM/EFFORT-Corrected Reflectance Data 9
- Partial Linear Unmixing of RTGC-Corrected Reflectance Imagery 11

Comparison of Field Burn-Severity Classification to Image Data 20

Operational Considerations 23

References 24

Abstract

The objectives of this project were to assess the potential of hyperspectral data to determine burn severity after wildfires and evaluate if the high spectral information makes it possible to detect water-repellency conditions of the soil. A burn-severity map helps prioritize rehabilitation efforts after a fire, reducing subsequent soil erosion and other problems. Generating such a classification requires developing a methodology to analyze the data and compiling a library containing spectra of burn-related materials.

Existing burn-severity classifications based on multispectral broadband remote sensing data have a few drawbacks that using higher spectral and spatial data can help solve. To analyze this more detailed information, two types of field data were collected in selected locations: plot data related to water repellency and burn severity, as well as field spectrometer data about surface materials that could be related to the image spectra.

The imagery data were analyzed using two methods. One method selects two bands of the short-wave infrared part of the electromagnetic spectrum to generate a simple ratio. This method is analogous to the normalized burn ratio that currently classifies broadband multispectral data but makes use of the additional narrow bands available in hyperspectral imagery, making it easier to target the wavelength used in the analysis. The second method, based on the mixture-tuned, matched-filtering algorithm, is a more traditional hyperspectral technique. The spectra comprising the signal present in a pixel are unmixed based on “pure” end-member spectra generated from material present on the surface.

The ratio method has the advantage of delivering results fairly fast compared to the second method because there is less need to preprocess the data accurately. However, just as the multispectral ratio does, this method produces a result for every pixel in the image whether it is related to the burn or not. The unmixing method results in less false positives and relates the classification of the data to materials present on the ground. Unmixing the data is, however, time consuming and very sensitive to preprocessing procedures such as atmospheric correction.

Relating the spectra to soil water-repellency conditions needs additional research. The orthorectification of the imagery was too coarse for accurate correlation with field data. But even with better rectification, this problem may be hard to solve. Determining water-repellency conditions often requires access to the soil just below the surface. Since visible and near-infrared wavelengths cannot penetrate the soil particles, remote sensing may not be the right tool. In locations where the fire has not burned the canopy, soil conditions cannot be assessed at all.

Introduction

For decades, rehabilitation crews have focused on mapping burn severity after wildfires. Burn severity varies depending upon the type of fuel present and the duration of the fire in a given location. Typically, burn severity is mapped as high, medium, or low. While these designations are useful for rehabilitation, they are difficult to map accurately. Recently, remote sensing in the form of airborne digital color-infrared photographs and multispectral satellite imagery have been used to map and infer burn severity. These tools can help delineate burn extent and vegetation condition after a fire; however, they have no direct link to burn severity. As new remote sensing tools become available, their capabilities must be tested—both on the ground and in the air—to determine how they can improve existing methods. New hyperspectral sensors show promise for improving our ability to collect direct measurements of burn severity.

This project addresses the needs of JFSP ***RFP 2001-2 Task 1***. In this project, hyperspectral airborne imagery and handheld field spectrometer data were collected following a large wildfire. The study's objectives were to collect and analyze information using these spectral data tools to determine how the next generation of sensors can help map and analyze burned areas. Funds from the project were used to 1) collect airborne hyperspectral imagery and field spectra; 2) prepare and analyze hyperspectral imagery using state-of-the art techniques; and 3) develop a final report and awareness poster highlighting the results of the study.

Objectives

Airborne hyperspectral sensors provide imagery in continuous bands for an area of the spectrum ranging from the visible to short-wave infrared (SWIR). Handheld spectrometers offer close-range information for the same spectral wavelengths and can help directly correlate ground-surface reflectance features and remotely sensed imagery. For this project, both ground and airborne-spectral data sets were collected to furnish direct estimates of on-the-ground burn severity. It is hoped that the spectral library of ground-surface features developed for this project—mainly burn-severity conditions—can be applied to future fires.

Specifically, the objectives of this project were the following:

1. To collect airborne hyperspectral imagery and field spectrometer data following a wildfire. Image-analysis techniques already developed for hyperspectral data were tested specifically for burn severity. Deliverables for this portion of the project include these:
    a) Georeferenced, mosaicked hyperspectral imagery;
    b) Field spectrometer data for representative burn-severity sites; and
    c) Classification algorithms for hyperspectral analysis of burn severity.
2. To develop a spectral library of burn-severity characteristics useful for image classification. Field spectral data were analyzed first to develop spectral correlations with burn-severity. Burn severity algorithms developed from field spectra were then applied to the hyperspectral imagery. Deliverables for this portion of the project include these:
    a) A postfire spectral library of various ground cover identified in the study area; and
    b) Classification of the hyperspectral images representing burn severity.

3. To develop quality assurance/control and image-acquisition protocols that can be used by BAER personnel. Deliverables for this portion of the project include these:

    a) An accuracy assessment of the burn-severity classification; and

    b) A report outlining protocols for future mapping efforts.

Study Area

The Hayman Fire was ignited on June 8, 2002, and by June 18 had burned more than 138,000 acres (Graham 2003). The fire was located within the South Platte River drainage on the Front Range of the Rocky Mountains between Denver and Colorado Springs, CO. Annual precipitation in this area is typically comprised of snowfall during the winter and high intensity showers during the summer. Since 1998, weather systems along the Colorado Front Range have brought below-normal precipitation and unseasonably dry air masses (Graham 2003). These drier-than-normal conditions in the predominately ponderosa-pine and Douglas-fir forests preceded the Hayman Fire.

The South Platte River flows from southwest to northeast through the interior of the burn. Cheesman Reservoir is a major impoundment on the South Platte River and is located near the center of the burn. The Denver Water Board owns and operates reservoirs like this one as an important water supply for the Denver metro area. Approximately 44 percent of the burned area drains into the South Platte River downstream of Cheesman Reservoir dam, while roughly 56 percent drains into either Cheesman itself or the South Platte River upstream of the reservoir. The Upper South Platte Watershed Protection and Restoration Project has identified the area as at risk for catastrophic wildfire (Graham 2003). Recent forest management has included firebreak development along Fourmile and Horse Creeks.

Data

Imagery Data

Data for this project included hyperspectral imagery collected by Earth Search Systems Inc.'s (ESSI) Probe sensor during August 2002. Analytical Spectral Devices (ASD) PRO-XR field spectroradiometer data and field-attribute data were collected during July 2002. It was not ideal that field data and imagery were not collected simultaneously because environmental and meteorological conditions change within short time periods. To add to the problem, the field spectra were collected at different locations from the detailed burn-severity field data. The end result was less-than-ideal field measurements, which is often the case with real-world remote sensing projects. However, putting the pieces together after the imagery was collected allowed the field data to become a guide during the analysis of the imagery data. Here is a description of the way the hyperspectral imagery was assembled.

Fourteen adjacent flight lines of hyperspectral imagery were collected by ESSI's airborne Probe sensor over the Hayman Fire study area. In remote sensing terminology, each flight line is called a hyperspectral image cube or data cube. Each data cube is 512 pixels across track, corresponding to a ground width of approximately 2.5 kilometers. The images contain approximately 28 kilometers of data along the track. The whisk-broom Probe sensor collects

information about the electromagnetic (EM) energy reflected from the surface in 128 contiguous spectral wavelength bands spanning the EM spectrum from 400 to 2500 nanometers. The spectral resolution of the bands is between 14 and 18 nanometers.

An on-board global positioning system (GPS) and inertial measurement unit (IMU) acquired geolocation information concurrent with the spectral data collection. The location information, together with 30-meter digital elevation models (DEMs), generated geographic lookup table files (GLT) for each flight line. This information is put into the image-analysis software to orthorectify the hyperspectral data cubes. The spatial resolution of the orthorectified data averages around 5 meters, varying slightly for each of the flight lines.

Field Data: Field Spectrometer Data

Bright target ground-calibration data were acquired through the cooperation of the USGS and its full-range ASD Fieldspec Pro field spectrometer at the granitic north shore of Cheeseman Reservoir (figure 1). The range of this spectrometer spans nearly the same part of the EM spectrum covered by the Probe sensor. The spectra collected at Cheesman Reservoir over bright, but spectrally bland, granitic rock were used to calibrate the image-sensor data to reflectance values. Field spectra of high and low burn-severity sites were collected on the ground as well as from a bucket truck. Cloud cover, reducing the amount of sunlight reaching the surface and indicative of higher water vaper present in the atmosphere, prevented the collection of field spectrometer data over the selected medium burn-severity sites. Water vapor

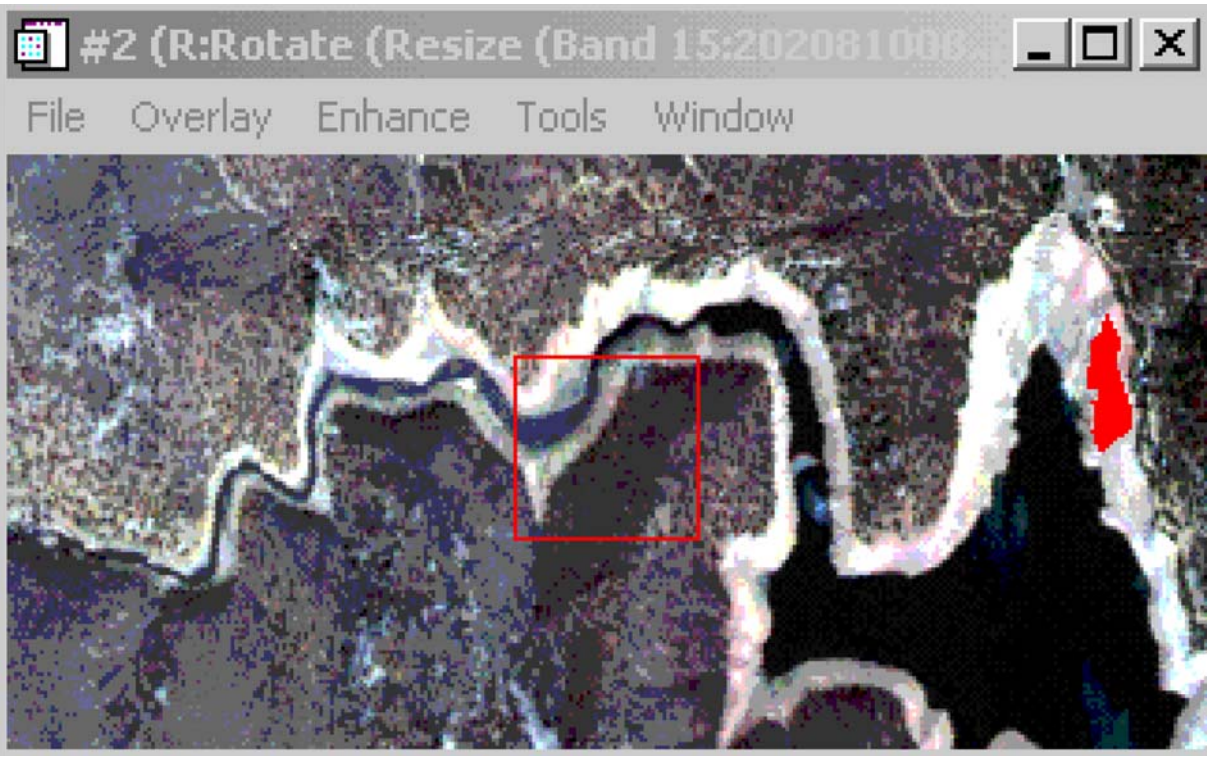

Figure 1—Location of the ASD field calibration site on the north shore of Cheesman Reservoir. A spectralon panel having well-documented reflectance in the 400 to 2500 nanometer region of the EM spectrum was used to calibrate the field spectrometer.

absorbs some of the EM signal. These conditions were too different from those present during the airborne data acquisition to make it possible to relate the two data sets. The field spectra acquired at the burn sites were used as a guide to generate the reference spectral libraries. One library was created for each flight line.

Field Data: Field Measurements

Ground validation data were collected at 182 field sites during the summer just after the fire. This information included data related to water repellency, the amount of litter and wood present, and the percentage of ash cover, as well as other field measurements required to determine burn severity.

Sampling Scheme

Approximately 60 sample points were selected in each of the three burn-severity classes (low, moderate, and high) as delineated by the BAER burn-severity map for a total of 182 sample points. East-west transects were located in visually homogenous burn sites at least 20 meters from roads. The transects were ideally 200 meters in length (figure 2), with central reference points (locations measured with a GPS unit, 50-centimeter resolution) at 0 meters (west end point), 50 meters, and 200 meters (east end point). Extending from each reference point were three 20-meter radials in the azimuthal directions of 0, 120, and 240 degrees.

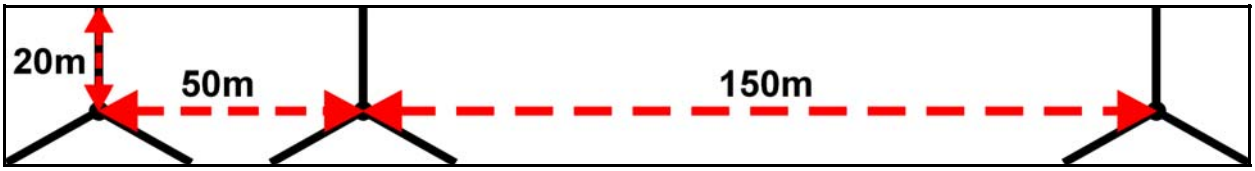

Figure 2—Two-hundred-meter field-plot transect layout.

The actual length of transects was between 50 and 400 meters (6 to 15 sample points each) as topography and uniformity of burn severity allowed. For example, in the low burn-severity class, there were 2 transects (50 meters long) with 6 points each and 6 transects (200 meters long) with 9 points each, for a total of 63 points along 8 transects. In the moderate burn-severity class, there were 7 transects (six 200-meter and one 50-meter) with 59 sample points (1 sample point was discarded due to poor data). In the high burn-severity class, there were 6 transects (five 200-meter and one 400-meter) with 60 sample points.

The sample points were located at the end of each of these radials. The spatial and directional layout of the transects and sample points was designed to encompass the variability of environmental data by sampling at short and long distances between sample points (35 to 435 meters apart), as well as sampling in different directions, so that variable positions on slopes would be captured. Each sample point was a circle with a 4-meter diameter in which all burn-severity and water-repellency measurements were made. The local aspect and slope percentage were measured using a compass and clinometer.

Burn-Severity Assessment

At each sample point, the burn severity was assessed by observing and measuring 24 variables indicating soil and vegetation conditions, as well as the local topography (Jain 2002). To reiterate, in this study, burn– severity primarily refers to the fire's effects on the ground surface and not the canopy vegetation. Visual classification of selected variables was measured in the 12.5 m^2 circle. The ground-cover percentage of new litter (postfire needle cast) was measured first since it was the uppermost layer. The smallest cover fractions were measured next; they were often grasses, forbs, shrubs, woody debris, stumps, and rocks. A value of 1 percent was recorded if there was a trace of the variable within the plot. The larger cover fractions—mineral soil, ash, litter, and humus (partially decomposed litter, not recognizable as needles or leaves)—were estimated last, and the cover percentage was summed to 100 percent. The burn percentage and degree of char (low, moderate, or high) of each of the cover components were estimated based on existing fire-effects literature (Parsons 2003; Ryan 2002; Ryan and Noste 1983).

The number of new tree seedlings (diameter at breast height [dbh] less than 25 millimeters) and saplings (dbh greater than 25 millimeters and less than 120 millimeters) was tallied. Green and burned trees (dbh greater than 120 millimeters) were counted and measured, and the char percentage was estimated. The depth of new litter, prefire litter, and humus was measured where they were present. An undisturbed soil sample was taken at the mineral soil surface (no deeper than 25 millimeters) at a random location within each plot to be analyzed for organic matter. A digital photograph was taken at each sample point for a visual reference encompassing the 4-meter circle.

Water-Repellency Tests

The Water Drop Penetration Time (WDPT) test was conducted at 11 evenly spaced points along a 0.5-meter line transect within each 4-meter circle. The surface ash and litter were swept aside to expose the mineral soil. At each point, a water drop was placed on the soil surface, and the infiltration time was measured. If the water drop remained on the surface for longer than five seconds, the soil was considered water repellent (DeBano 2000; Letey and others 2000). The degree of water repellency was assessed by measuring the persistence of the drop on the soil surface for up to 360 seconds. Water repellency was divided into three classes by the average time it took for the drop to infiltrate per plot: low (0–60 seconds), moderate (61–180 seconds), and high (181–300 seconds) (Dekker and Ritsema 1994).

Minidisk infiltrometer (MDI) tests were performed on a line parallel to and within 200 millimeters directly above or below the WDPT test line. The field-portable MDI had a constant pressure head of five millimeters with a 31 millimeter–diameter porous disk. The graduated cylinder body allowed cumulative infiltration per time period to be read directly. The MDI was filled with water and placed on the exposed soil surface at four evenly spaced locations along the line. To minimize lateral flow, soil or ash were not allowed to touch the sides of the porous disk. The time to the start of infiltration was noted, as well as the volume of water that then soaked into the soil within the first minute.

Atmospheric Correction Methods

Typically, remote sensing radiance is converted to reflectance to relate field measurements to hyperspectral image pixels. All airborne and spaceborne remote sensing instruments measure the upwelling radiance that arrives at the sensor. This radiance results from solar irradiance, two-way transmittance and scattering of the atmosphere, and reflectance of the surface. It is this reflectance of surface material that remote sensors concerned with researching the characteristics of ground cover want to study (Gao and others 1993; Analytical Imaging and Geophysics 2002).

An initial reflectance data set was processed by ESSI. These data were adjusted for radiance by applying the ATREM code (Gao and others 1993, 1999), followed by an EFFORT polishing to remove artificial spikes introduced by the ATREM correction (Boardman and Huntington 1996; Boardman 1998a; Clark and others 2002). Because of the EFFORT smoothing, it was not possible to apply the radiative transfer ground-controlled (RTGC) calibration for which the USGS had collected the ground spectra.

To improve the image-processing possibilities, a second set of reflectance data for all but two of the data cubes was provided by the vendor. These data were eventually provided at a later date. Atmospheric correction was accomplished using ACORN (Analytical Imaging and Geophysics 2002) without any additional artifact suppression. Calibration of the nonsmoothed reflectance data was refined based on a multiplier calculated from the differences between the mean image-reflectance spectrum over the area where the ground-truthing ASD spectra were collected and the average ASD spectrum. Then the average ASD spectrum was corrected for the spectralon reference-panel absorption feature and resampled to the bandwidth wavelengths of the Probe sensor (Clark and others 2002).

This must be done because the spectralon panel is a bright calibration target with well-documented reflectance in the 400 to 2500-nanometer region of the EM spectrum. The field spectrometer is calibrated against the panel immediately before field spectra are collected. Because the panel has an absorption feature near 2.13 micrometers, this feature needs to be corrected in the field spectra. In addition, to compare the field spectra to the image spectra, the narrower spectral bandwidths of the field spectrometer need to be resampled to the same spectral resolution as the image spectra.

The ATREM/EFFORT, ACORN, and RTGC reflectance spectra of the same pixel extracted from the image cube at the calibration site are compared in figure 3. Granite and ash are used in the comparison; both locations contain no live vegetation.

The two data cubes with missing ACORN-generated reflectance data were provided at a later date and therefore dealt with separately. Comparing ACORN reflectance spectra of the same geographic location on adjacent flight lines (lines 7 and 8) indicates the first set of ACORN reflectance data was processed with different input parameters from the second set (figure 4). Since flight lines 8 and 7 contain pixels corresponding to the Cheesman Reservoir ground calibration site, a different set of multipliers was calculated and applied to the new ACORN reflectance spectra (figure 5).

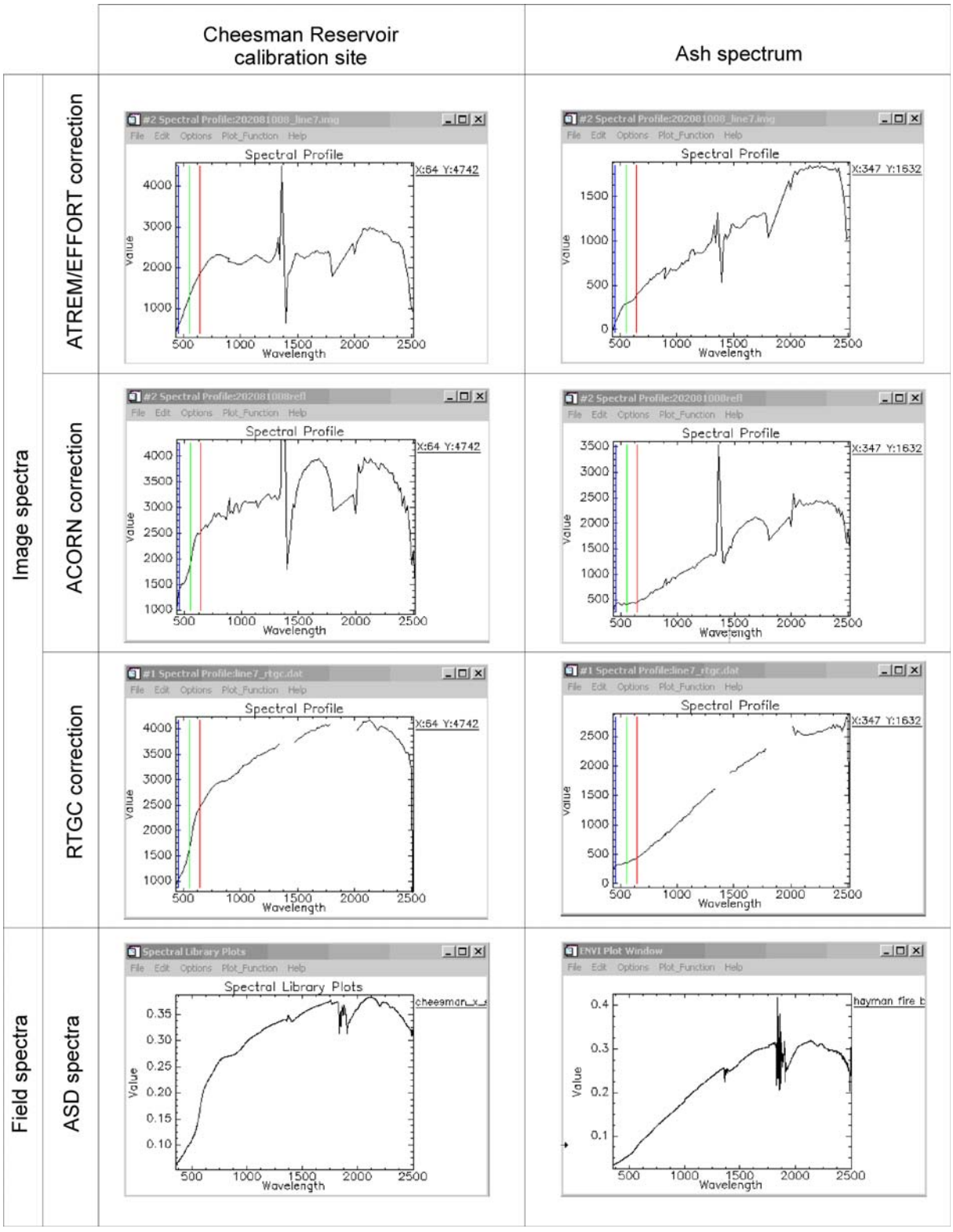

Figure 3—Comparison of reflectance spectra representing granite at the calibration site near Cheesman Reservoir *(left)* and a sample representing ashes *(right).*

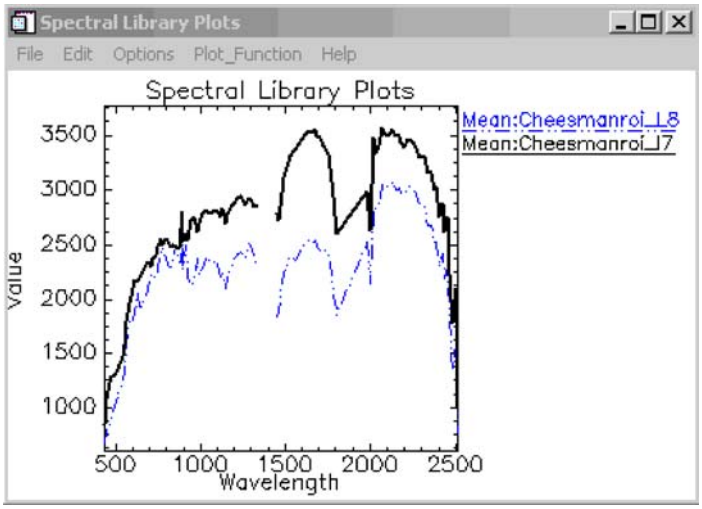

Figure 4—ACORN-calibrated reflectance spectra representing the Cheesman Reservoir calibration site extracted from flight line 7 *(solid line)* and flight line 8 *(dash dot).* Note the differences in the visible near-infrared (VINR) region of the spectrum where the ACORN-generated reflectance from line 7 is less "spiky."

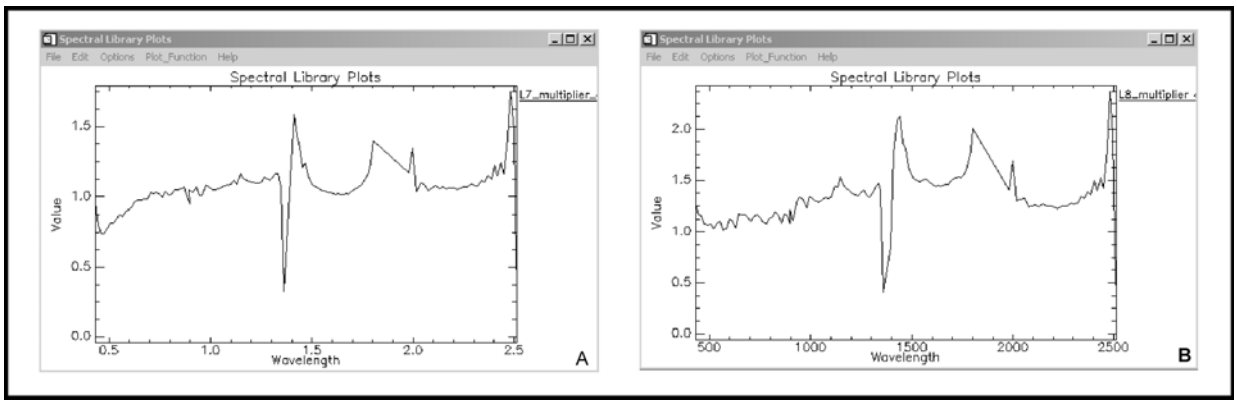

Figure 5—Comparison of multiplier correction derived from flight line 7 *(A)* and flight line 8 *(B).* The numbers derived from line 7 were applied to calibrate the ACORN-generated reflection spectra for all lines except 3 and 8, for which the multipliers from line 8 were used.

As is evident from this discussion on atmospheric correction, data processing can be time consuming and technical. Because of the enormity of the data set (14 flight lines with 128 spectral bands) and potential difficulties receiving data from vendors, careful planning needs to be done before image data are acquired.

Data Analysis

Two analysis procedures were applied to the hyperspectral data cubes. First, a process called band-ratio analysis was performed on the ATREM-corrected reflectance data. The ATREM-corrected data set was the first one received and therefore available in the early stages of the project. Once the second set of ACORN atmospheric-corrected data was delivered, RSI's ENVI

mixture-tuned, matched-filtering (MTMF), partial-unmixing algorithm was applied to the RTGC reflectance data (Boardman 1998b). The ATREM-corrected reflectance data were used in the first phase due to time constraints. That way some analysis could be completed while waiting for the nonsmoothed reflectance data.

SWIR-BR Band Ratio Generated from ATREM/EFFORT-Corrected Reflectance Data

During the first phase of this project, the normalized burned ratio (NBR) technique developed by the USGS (Key and Benson 2002) was adapted from multispectral to hyperspectral imagery to make use of its narrower spectral bandwidth. The NBR method is used on multispectral satellite imagery by the U.S. Forest Service to map burn severity (Orlemann and others 2002). This process has the advantage of being simple to apply and easy to understand.

The NBR method uses Enhanced Thematic Mapper (ETM) bands 4 and 7 to classify multispectral data for burn severity (Key and Benson 2002). Using the hyperspectral data, the input wavelength ratio of 2165 and 1655 nanometers was selected. These wavelengths are in a similar location to the ones used in the NBR method but are much narrower in the hyperspectral imagery. These bands were selected based on observations from the field spectra and because the spectral characteristics of dead woody vegetation are expressed in the SWIR part of the spectrum. Typical spectral characteristics of healthy green-leaf vegetation are found in the visible near-infrared (VNIR) part of the EM spectrum (Elvidge 1990; Roberts and others 1993).

Figure 6 shows four spectra extracted from flight line 7, which encompassed the Cheesman Reservoir calibration site. These four materials are commonly found following forest fires: green vegetation, brown scorched vegetation, ashes, and bare soil/rock. This figure also shows the location of the two bands chosen for the band-ratio process. The differences among the four chosen spectra are quite apparent in this example.

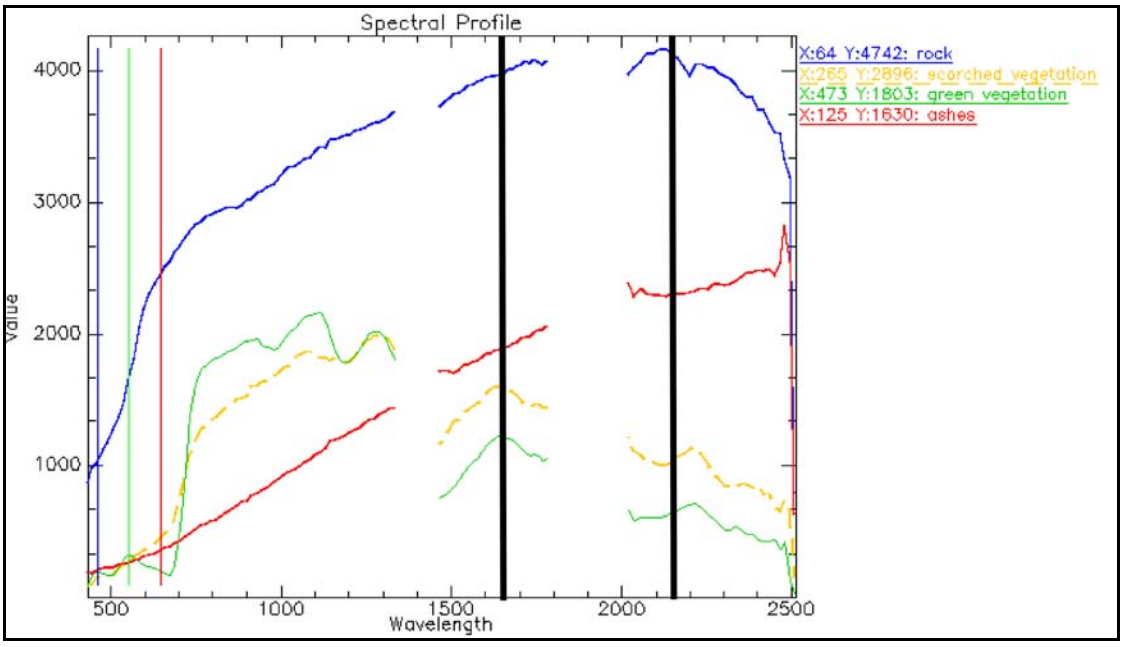

Figure 6—Examples of RTGC-corrected reflectance spectra representative of surface materials following a forest fire.

The results of the SWIR burn-ratio (SWIR-BR) process show that most BR values vary between -0.5 and +0.5. The lower values characterize unburned vegetation while higher values indicate burned vegetation, soil, and ashes. Outliers on both extremes of the selected range were generated, but these were more indicative of problems with the data than expressions of burn severity.

The floating-point results of the SWIR-BR ratio were categorized and reclassified into four integer classes: no burn/underburn and low, moderate, and high burn severity. Because of differences in data calibration from one flight line to the next, slightly different break points were assigned to each of the burn-severity categories on the different flight lines. Minimum and maximum values of the SWIR-BR process are shown for each flight line at each end of table 1.

Assigning cutoff values for each of the burn-severity categories was subjective and based on a combination of 1) visual inspection of the initial classification, and 2) a review of the breaks in the statistical distribution of the BR values. The classification was checked by randomly evaluating image spectra in each of the classes. Once the break points were chosen, each BR image was georeferenced to UTM zone 13 NAD 83 using the geolocation files provided by the vendor. As discussed earlier, once georeferenced, the pixel size for each of the flight lines was around 5 meters but varied from one flight line to the next.

Table 1—Burn-severity breaks for each flight line. Negative values characterize unburned vegetation while positive values indicate burned vegetation.

	Severity					
	Unburned		Low	Medium	High	NDVI
	min	green	yellow	orange	Red (max)	cutoff
Line 1	-0.78004807	-0.07	-0.05	0.03	0.384615392	0.14
Line 2	-7.381219592	-0.07	-0.05	0.03	6.650485516	0.1
Line 3	-1.96653968	-0.08	-0.025	0.027	5.081712529	0.1
Line 4	-0.5	-0.08	-0.025	-0.0003	0.305637986	0.125
Line 5	-0.483542323	-0.15	-0.05	0.0	0.407371253	0.1
Line 6	-0.777740893	-0.051	0.05	0.084	0.386949927	0.15
Line 7	-0.494579105	-0.1	0.04	0.11	0.673469365	0.1
Line 8	-0.629605261	-0.2	-0.07	0.035	0.536842108	0.05
Line 9	-0.544270862	-0.03	0.07	0.13	0.623188376	0.15
Line 10	-0.664751797	-0.13	-0.05	0.05	1.294117689	0.1
Line 11	-0.58601188	-0.11	-0.04	0.07	0.580952406	0.1
Line 12	-0.593080972	-0.1	-0.05	0.065	0.573799491	0.1
Line 13	-0.630343944	-0.17	-0.05	0.07	0.536094666	0.1
Line 14	-0.567901254	-0.1	-0.05	0.1	0.224270359	0.1

One point worth nothing is that even after georeferencing, the location of one pixel in the overlapping zones of two flight lines could be off by as much as 30 meters. This made it difficult to precisely compare the field spectra and field data to the pixels in the hyperspectral image. Finally, the georeferenced, calculated SWIR-BR was reclassified into the four burn-severity categories. Reclassifying the image into four categories produces a smaller file size for each flight line, making it possible to mosaic the lines into a single classified image. The individual flight lines were then resampled using the nearest neighbor algorithm to a common pixel size of 5 meters.

To improve upon the SWIR-BR classification, a normalized difference vegetation index (NDVI) (Rouse and others 1974), using wavelengths 646 and 826 nanometers (bands 15 and 27), was applied to mask areas containing water, cloud shadows, bare soil, and invalid data. The objective was to eliminate as many pixels as possible that contained materials unrelated to forest burns but that had a SWIR-BR value similar to the high burn-severity category. The NDVI was an efficient way of masking pixels with very low NDVI values (water, clouds, invalid data) from the SWIR-BR. Soils and rock have NDVI values similar to those generated by burned materials, which made it more difficult to mask the soil and bare rock from the burn-severity classification. The NDVI results were scene dependent as well. SWIR-BR categories with an NDVI less than 0.1 (see table 1) were assigned to an "other" category (figure 7).

In summary, the SWIR-BR method is fast and does not require extensive fieldwork to characterize and compile reference spectra. The disadvantage is that the cutoff values for the different classes change for each of the data cubes. This method still requires masking to eliminate nonburned land cover and its data. While the final classification produces a burn-severity map, it does not utilize hyperspectral imagery's full potential to characterize which material is represented in a pixel or quantify the abundance of a certain material.

Partial Linear Unmixing of RTGC-Corrected Reflectance Imagery

To exploit further the spectral information available, hyperspectral data should be analyzed with techniques developed specifically for it. Typically, a single image pixel does not contain a single surface material but a mixture. Even when dealing with high spatial-resolution data, a single pixel often represents a mixture of materials.

The spectrum extracted from such a pixel mixes the spectra of all the different materials in that image pixel. This mixed spectrum retains some of the characteristic features of the "pure" spectra, although they are diminished. Often features typical for a specific material, such as a mineral, or a similar group like vegetation are fairly narrow, even ten(s) of nanometers. They are generated because of ways incoming EM energy interacts with different chemical bonds in the surface materials. Broadband multispectral data does not pick up many of these features. Because hyperspectral data possesses high spectral information, specific analytical techniques can characterize and distinguish these features from one another.

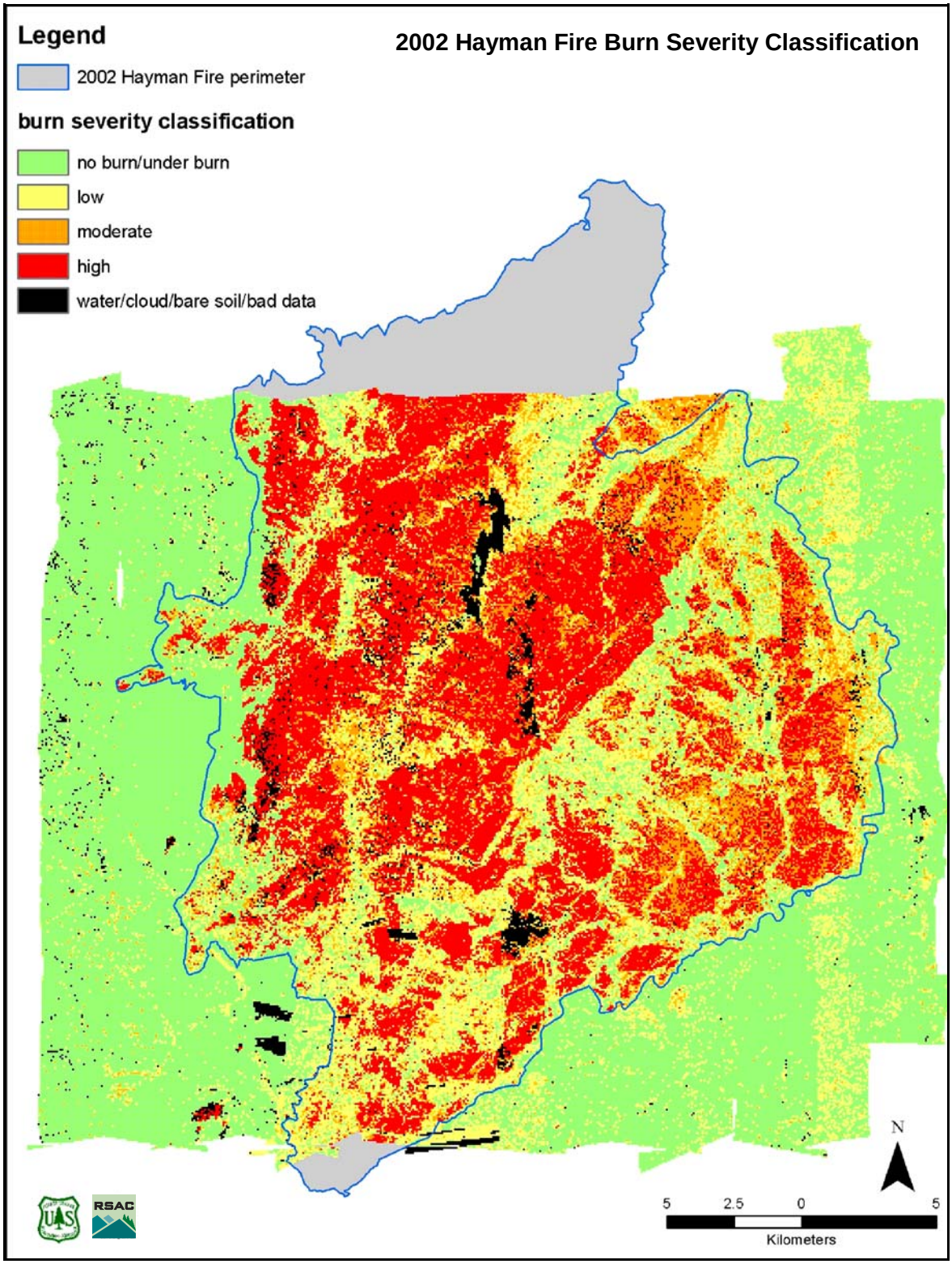

Figure 7—Classification of the Hayman Fire using the ratio-generated SWIR-BR image. The northernmost portion of the fire was not covered by imagery.

Because of hyperspectral spectra's high information content, it is possible to unmix the signature of each pixel and estimate its individual components. In its most essential form, the signal in each image pixel can be expressed as a linear combination of all the purest spectra, known as purest end members, in the image. Once the end members are known, linear unmixing of the data indicates what fraction of the pixel is comprised of each material (Adams and others 1986). Making this process work well requires good reference spectra.

These reference spectra can be obtained from existing spectral libraries, collected in situ with a field spectrometer, or extracted from the image cubes. To be able to compare them to library reflectance spectra, the image spectra have to represent the surface material and therefore be uninfluenced by the illumination source, any atmospheric gasses, scattering, and, ideally, adjacency effect problems, all of which can modify the pixel signal received by the sensor.

The RTGC-corrected reflectance data were reduced with ENVI's minimum-noise-fraction (MNF) transformation to 20 MNF bands. A library of reference spectra representing ashes, soil/rock/dirt road, green vegetation, and scorched vegetation was created for each data cube. These spectra do not correspond to the traditional burn-severity classes. However, burn severity is traditionally measured on the ground according to parameters that are not always visible from the surface layer, such as changes in the vegetation and litter unconsumed by fire, changes in mineral soil, water repellency, and root conditions (DeBano and others 1998). Residual ashes often hide these characteristics. While the soil is accessible to field investigators, the sensor cannot see through the overlaying materials from the air.

Another parameter used to determine burn severity is the amount of postfire litter cover, needles on the ground, organic material, etc. When hidden under a tree canopy that still has crown cover, this amount is also hard to evaluate from airborne data. Vegetation cover present before a forest fire also influences the burn-severity classification. For example, grass versus forest cover affects burn severity. This cannot be assessed with postfire images alone. Additional factors such as erosion potential cannot be determined from postfire hyperspectral images alone, either. Some of these factors can be modeled in a GIS by integrating ancillary data with the results of the image analysis.

Linking image and field spectra to the burn-severity classes ultimately requires more detailed research at the field level to establish the relationship to the image data. Based on information in the imagery, a slightly different approach from the field-based burn-severity classification was required to assess the burn scars. This approach focused on the assessment of individual components of the scorched landscape after a fire: green vegetation, scorched vegetation, ash, and bare soil. Bare soil was included in the analysis since the vegetation that would prevent soil erosion is no longer present at many locations after a fire sweeps through an area.

All the libraries, one generated for each flight line, were transformed to principal component space using the noise statistics derived from the MNF transformation of the corresponding image. Creating a different library for each image eliminated problems with residual atmospheric effects after the RTGC calibration. Since these lingering effects were present in the library as well as the image data, this process minimized their effect on the unmixing. The disadvantage of this method is that a slightly different library had to be used for each of the data cubes, reducing the consistency from one flight line to the next.

The first 20 bands of each MNF-transformed data cube were partially unmixed with the MTMF algorithm available in ENVI. One of the major advantages of partial unmixing compared to linear unmixing is that not all the end-member spectra in a hyperspectral image need to be included in the analysis. Spectra of materials not corresponding to library spectra are suppressed and processed as background.

ENVI produces two gray-scale output images for each input spectrum: a matched-filter score and an infeasibility score (figure 8). The matched-filter score (MF), generally varying continuously between 0 and 1, indicates how well the image pixel compares to the reference spectrum and measures how abundant a certain material is in that image pixel. The infeasibility score (IF) shows how likely or unlikely the match is. Pixels that combine a positive MF score (higher values) with a low IF score (lower values) contain the best matches. Both these scores can be graphed in a 2-D scatterplot (figure 9).

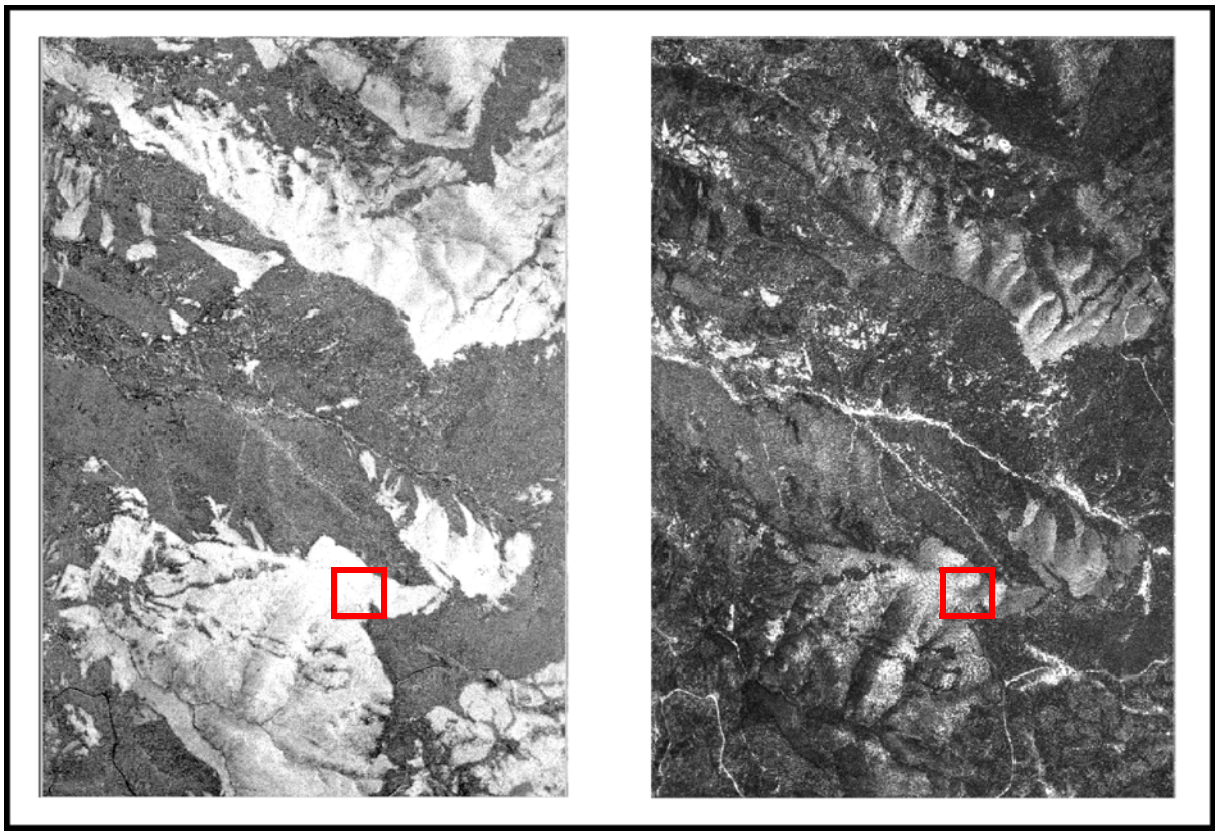

Figure 8—Subset of line 7 showing MF score for ashes *(left)* and IF score for ashes *(right)*. Areas that are lighter colored on the left and darker colored on the right are most likely to contain ash.

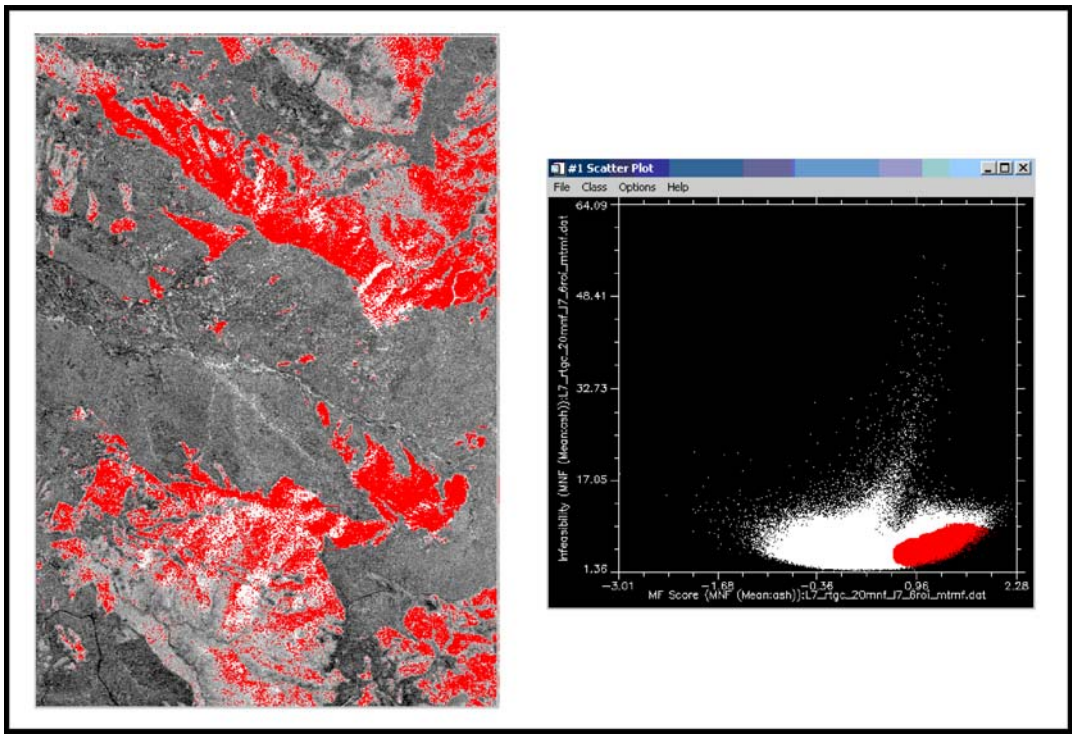

Figure 9—Subset of line 7 showing MF score for ashes with red pixels corresponding to red region of interest (ROI) delineated on the 2-D scatterplot *(right).* The *X* axis graphs MF scores of all the pixels of the image on the left plotted against the IF scores on the *Y* axis.

Once each data cube was unmixed, the resulting scores were georeferenced using the GLT files, and all the flight lines were mosaicked into a single image. This image was nearly 2.5 gigabytes in size and contained 12 continuous gray-scale bands: an IF and MF band for each of the component spectra of ash, scorched vegetation, green vegetation, soil, rock, and dirt road.

Since the results of the partial unmixing are continuous data, each band can be input into a red-green-blue (RGB), color-composite image as seen in figures 10 and 11. Here red represents the result of unmixing the ashes, blue corresponds to the bare soil/rock/dirt, and the scorched vegetation is green. Although the RGB image shows where the fire reduced the forest to ashes or the trees were not completely consumed, it does not take into account the IF score (figure 12). The IF image score can generate masks for the MF image. These masks can help eliminate unlikely occurrences of individual components.

An alternative way of representing the information in the two output images is to classify the data into discrete classes representing burn categories (figure 13). Unfortunately, the image containing the 12 output scores (6 MF bands and 6 IF bands) was too large for the image-processing software, Leica Imagine, to handle. The data set was reduced by classifying rock, bare soil and dirt roads into the same spectrum. Because of the similarity among the soil, rock, and dirt road spectra, their output scores from the partial unmixing were similar. The results of the soil reference spectrum were used to classify the three materials. The final interpretations—the RGB composite or the classified image—can be incorporated into a GIS or used for modeling.

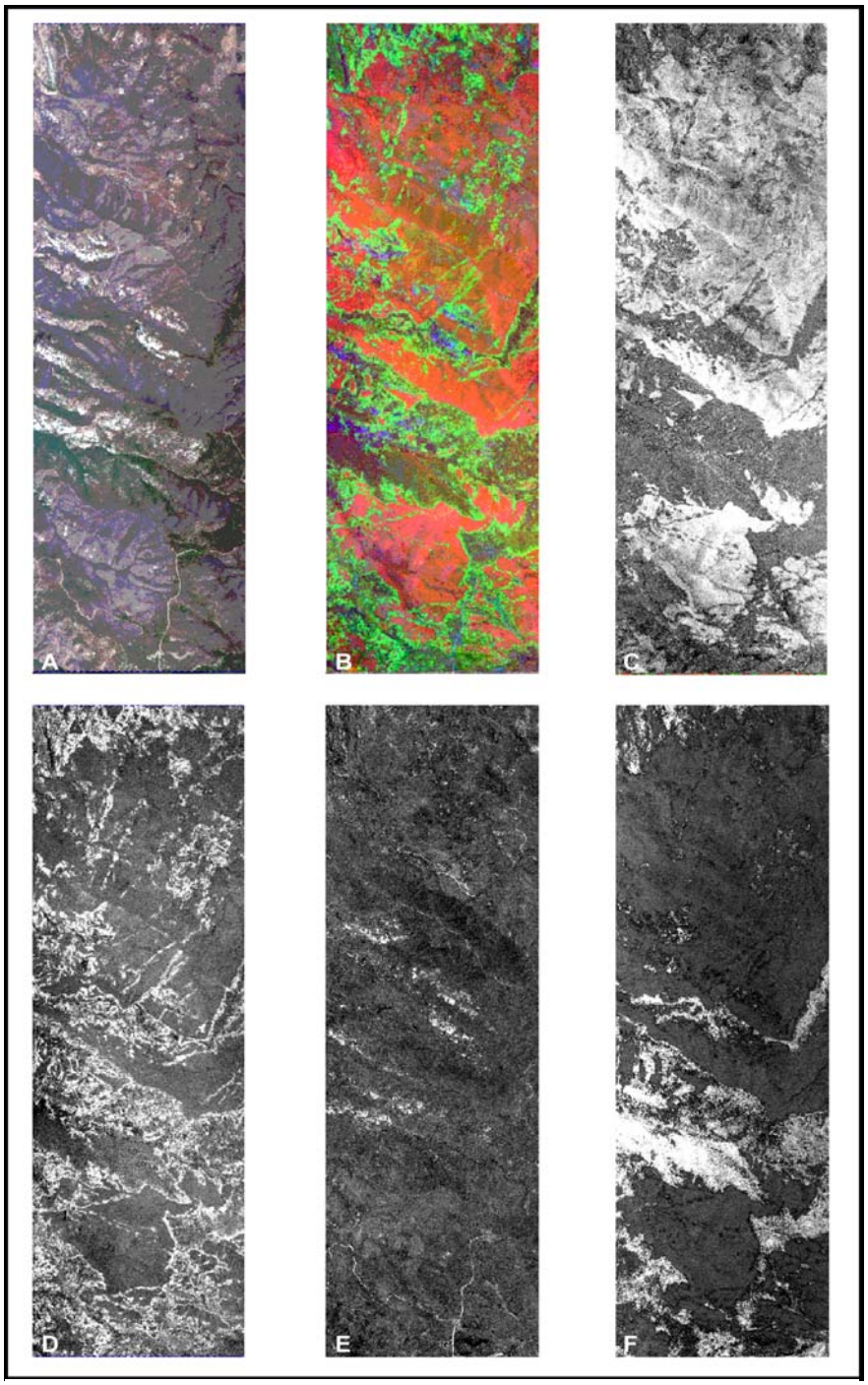

Figure 10—Comparison of hyperspectral imagery and derived products for portion of flight line 7: *A)* natural-color representation of the visible wavelengths corresponding to the blue, green, and red wavelengths of the EM spectrum; *B)* RGB composite of the MF score for unmixed ashes (red, *C),* scorched vegetation (green, *D),* and soil/rock (blue, *E); C,D,E*) the individual gray-scale images of the three components in figure 10B; *F*) MF score for green vegetation, which shows as dark pixels in the RGB composite of figure 10B. Lighter-colored gray-scale pixels correspond to closer matches with the reference spectra.

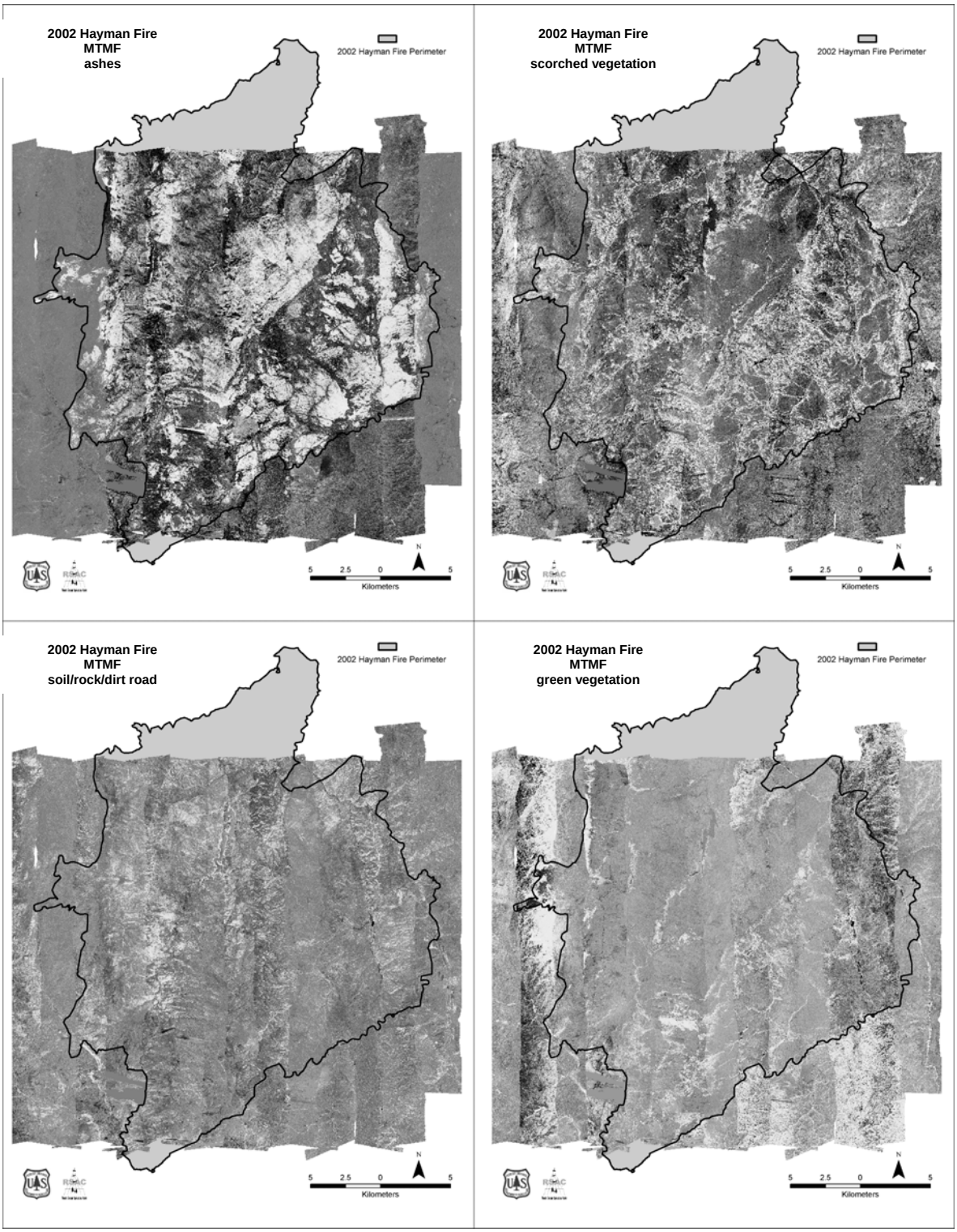

Figure 11—Hayman fire gray-scale images showing the mosaicked MF scores derived from partial unmixing of the individual data cubes for ashes *(upper left),* scorched vegetation *(upper right)*, soil/ barren rock/dirt roads *(lower left),* and green vegetation *(lower right).* Brighter pixels correspond to higher MF scores and are more likely close matches. The first three images are combined in figure 12.

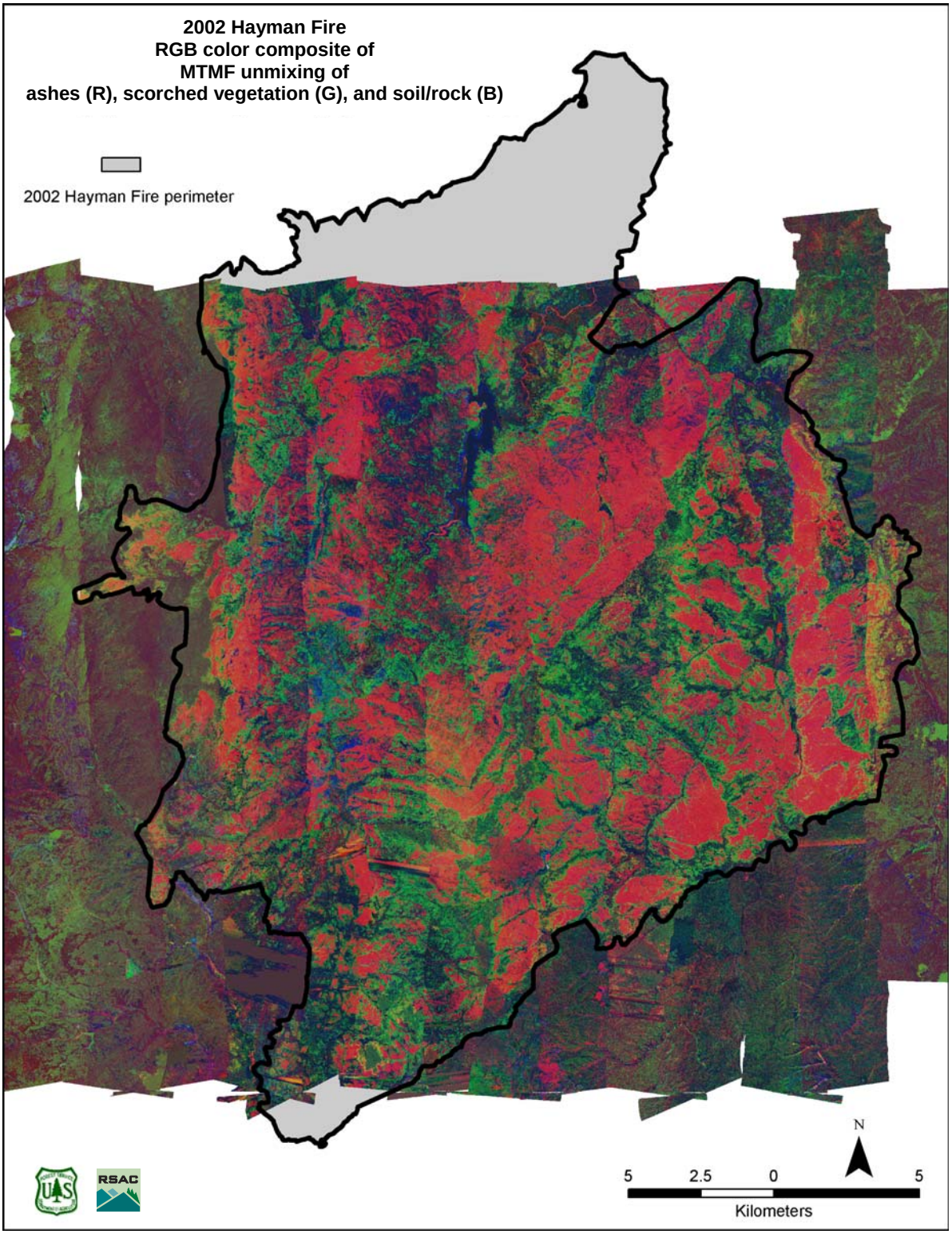

Figure 12—Hayman Fire RGB histogram, enhanced color-composite image of MF scores derived from partial MTMF unmixed mosaic of ashes (red band), scorched vegetation (green band), and soil/rock (blue band).

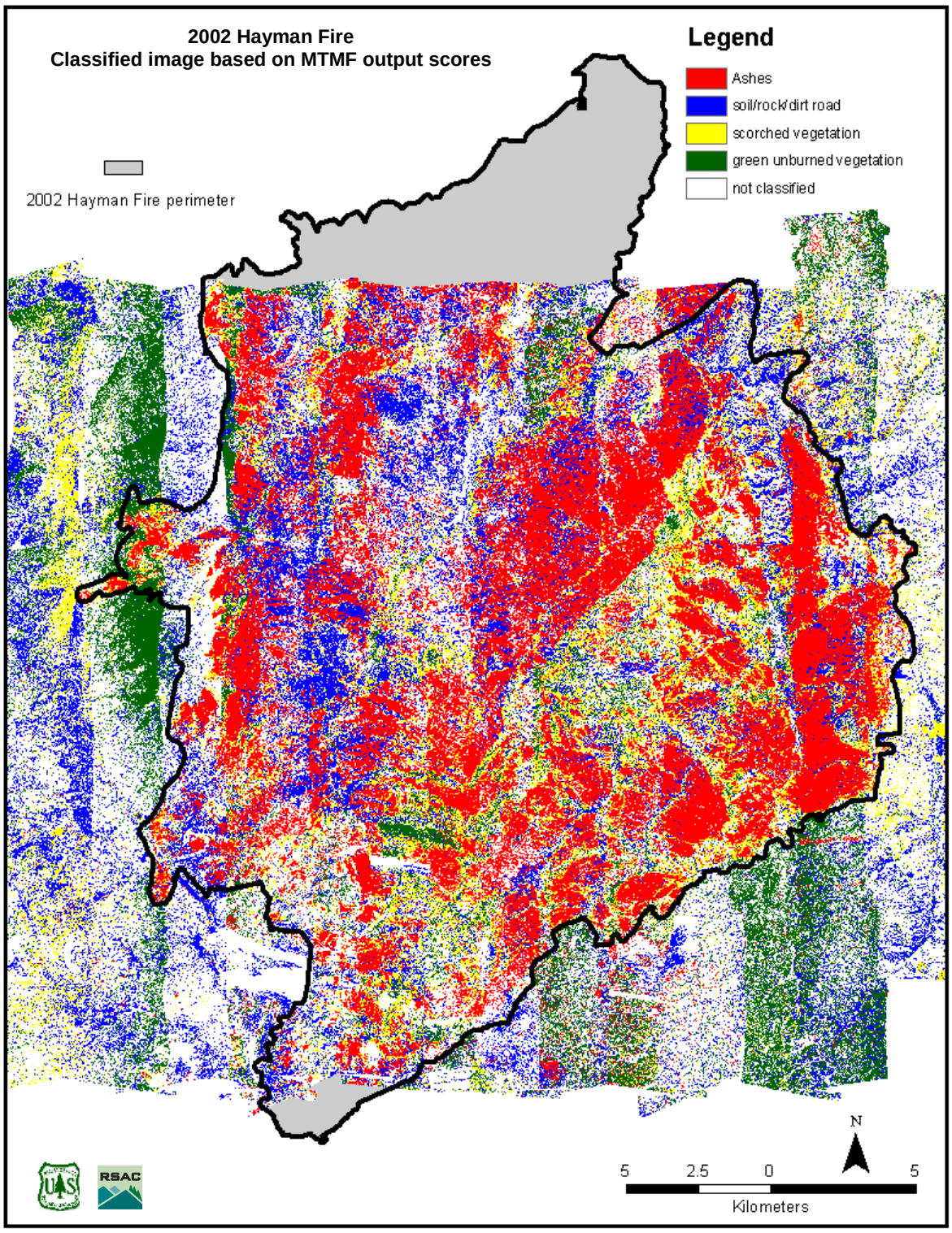

Figure 13—Classified results of the Hayman fire hyperspectral data based on cutoff values from both the MF and IF scores of the ashes, scorched vegetation, soil/rock, and unburned, green vegetation.

Each method of representing the results has advantages and disadvantages. The continuous RGB color composite reveals gradual changes in the amount of each material, but its file size is larger, and the final image requires color enhancement to display it best. Also, to use this image in a GIS model, it most likely needs to be reclassified into a meaningful set of categories. Conversely, the thematic classified image is smaller in file size and easier to interpret because it has been classified into discrete categories, but it contains less information.

Although the RGB color composite and the classification of the unmixing results deviate from the established procedure of categorizing postburn remote sensing images into low, moderate, and high burn severity, the results are useful since they indicate which material and how much of it are actually present. Comparing the results of the band-ratio and unmixing techniques indicates that the unmixing technique identified fewer false-positive pixels as part of the burned area—either ashes or scorched vegetation. Partial unmixing did not require generating a mask to exclude ratio values representing materials unrelated to the fire, such as clouds, water, and rock outcrops. Pixels containing these materials were classified as moderate to high burn severity using the ratio technique but show up as either fairly dark pixels in the RGB composite—representing very low values in the MF scores—or as unclassified in the unmixing classification.

Comparison of Field Burn-Severity Classification to Image Data

The next series of illustrations are highly detailed screen images of the RGB composite in figure 14 with the color-coded field locations used to determine burn severity on the ground. Low burn-severity locations appear in green, moderate in yellow, and high in red. Each pixel in the RGB image corresponds to 5 meters on the ground. Ideally, low burn-severity sites characterized in the field should correspond to either dark pixels or bright, light green ones in the image. Moderate burn-severity sites should plot as either bright, light green pixels or orange/yellowish ones, the color generated by mixing red and green. Lastly, high burn-severity sites should correspond to bright red pixels if no soil is present or blue to magenta ones, depending on how much bare soil is present and thus mixed into the pixel (table 2).

As can be observed from the illustrations, the field-collected burn-severity data does not always correlate with the expected corresponding colors in the RGB composite. This needs further investigation, but here are some possible reasons why the relationship may not be straightforward:

- Even if the registration of the field locations to the imagery were perfect, these locations do not always center on a pixel. In cases where the field location coincides with the corners of more than one pixel, which one should be used? This becomes more important in areas where the burn severity can very. These areas are the more speckled ones in the imagery.
- Not having an exact georegistration of the image data is a factor as well. The location of the ground data may be off by several pixels, particularly at the edges of a flight line.
- Using different libraries of reference spectra to unmix each of the data cubes most likely influenced the results.

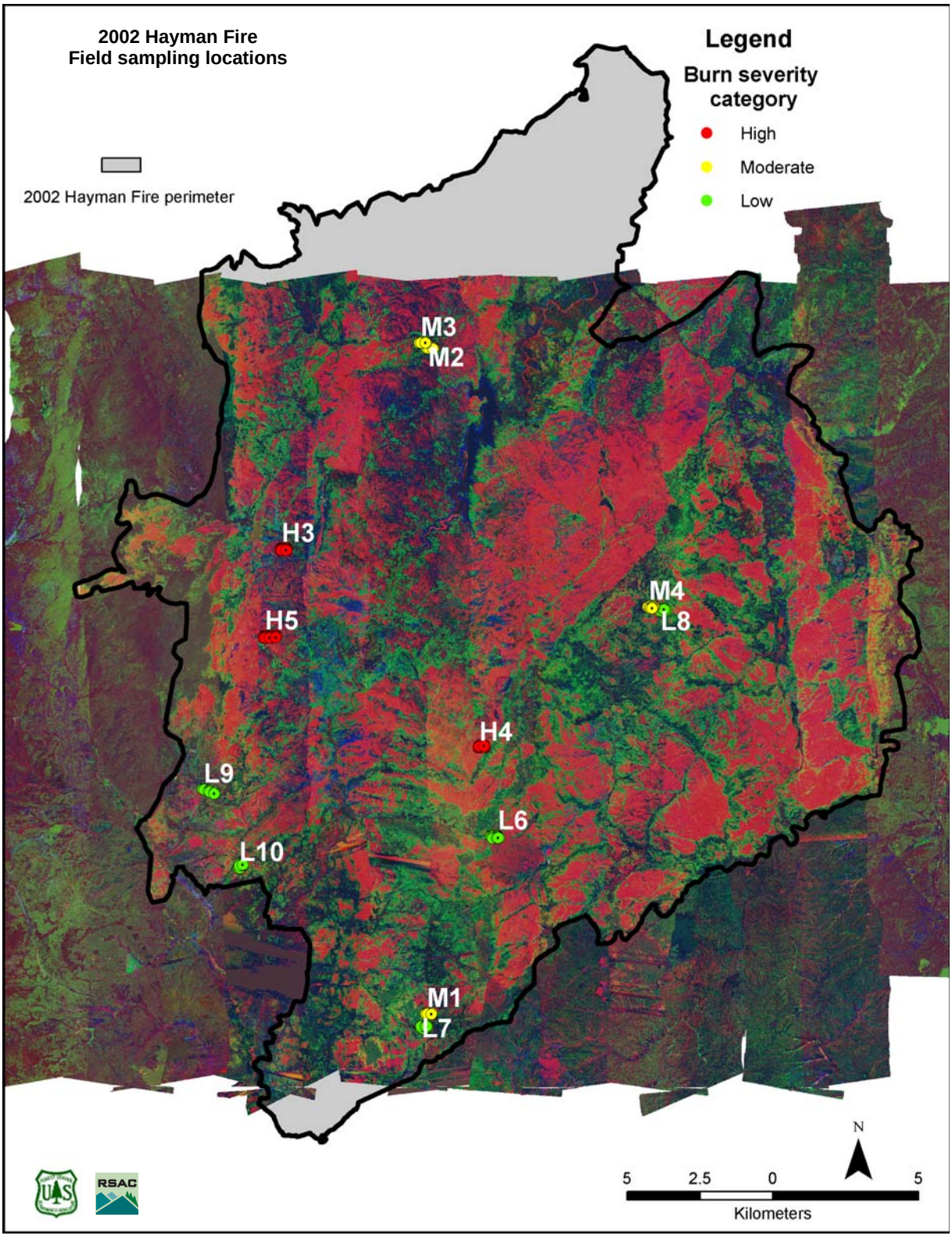

Figure 14—Overview of the locations of field sampling sites superimposed on the RGB composite depicting the unmixing results.

Table 2—Comparison of field-determined burn-severity categories to RGB composite image colors.

Burn-Severity Category	RGB Color R: Ashes, torched vegetation G: scorched vegetation B: rock, soil, or dirt road	RGB Color Explanation
High	Red	Represented by high ashes and torched-vegetation MF score
	Blue	Only soil is present (no ashes or vegetation): high-soil MF score displayed by the blue band
	Magenta	Both ashes and soil are mixed
Moderate	Bright green	Favorable MF score for scorched vegetation
	Orange	Mixture of scorched vegetation (represented by green band) and ashes (represented by red band)
Low	Dark to light green	Most of the canopy is not affected by the fire. This green canopy cover will shield the burn scars closer to the forest floor. When some of the lightly burned vegetation can be detected by the sensor signal, the spectra resembles the scorched vegetation.
Unburned	Dark	No good matches (i.e., high MF scores) in either of the three individual bands

- Not collecting field spectrometer data at the same locations where burn severity was characterized in the field made it difficult to correlate the field spectra to the ground data, especially since no detailed data measurements were taken at the field spectrometer sites. Because of weather problems, no field spectra were collected at moderate burn-severity sites at all, making this class even harder to assess from the imagery.
- Nonground-penetrating remote sensing data cannot assess the same subsurface parameters as the field investigator can. Some of these factors are very important to determine burn severity.
- Finally, the hyperspectral data were acquired two months after the fire was controlled. Rain from a few big storms occurring between the fire and data collection might have caused some runoff, changing conditions on the ground.

The correlation between the high burn-severity category and the unmixing results is fairly good, especially for sites H4, H3, and most of H5, indicating this promising technology merely needs further fine-tuning.

Operational Considerations

The analytical results of this project indicate that hyperspectral image data are useful to evaluate postburn forest areas. To use this type of data for rehabilitation and erosion control after a fire, however, a few operational issues need to be addressed.

Hyperspectral data are not easily acquired immediately after a fire. In areas requiring large coverage, close attention must be paid to the data quality and consistency from flight line to flight line. Care should be taken when writing contracts that vendors are required to provide metadata and document all processing steps before giving the data to the user.

File size is another important consideration. Computers are getting faster and storage devices larger, but processing this amount of information in a timely manner is still an important issue at this time. Additional research is required to generate a single analytical procedure that can be used repetitively from flight line to flight line and, ideally, from fire to fire. Generating a different reference library for each flight line was necessary to deal with data inconsistencies in a timely manner, but unfortunately this decision generated a final mosaic that was not entirely “seamless.”

References

Adams, J.B.; Smith, M.O.; Johnson, P.E. 1986. Spectral mixture modeling: a new analysis of rock and soil types at the Viking Lander 1 site. Journal of Geophysical Research. 91(B8): 8098–8112.

Analytical Imaging and Geophysics LLC. 2002. ACORN 4.0 stand-alone version. Boulder, CO. 64 p.

Boardman, J.W. 1998a. Post-ATREM polishing of AVIRIS apparent reflectance data using EFFORT: a lesson in accuracy versus precision. In Green, R.O., ed. Summaries of the seventh annual JPL airborne earth science workshop, January 12–16, 1988, Pasadena, CA. Pasadena, California: Institute of Technology: vol. 1, 53.

Boardman, J.W. 1998b. Leveraging the high dimensionality of AVIRIS data for improved subpixel target unmixing and rejection of false positives: mixture tuned matched filtering. In Green, R.O., ed. Summaries of the seventh annual JPL airborne earth science workshop, January 12–16, 1988, Pasadena, CA. Pasadena, California: Institute of Technology: vol. 1, 55.

Boardman, J.W.; Huntington, J.F. 1996. Mineral mapping with 1995 AVIRIS data. In Summaries of the sixth annual JPL airborne earth science workshop. JPL Pub. 96-4, Pasadena, CA: Jet Propulsion Laboratory: vol. 1, 9–11.

Clark, R.N.; Swayze, G.A.; Livo, K.E.; Kokaly, R.F.; King, T.V.V.; Dalton, J.B.; Vance, J.S.; Rockwell, B.W.; Hoefen, T.; McDougal, R.R. 2002. Surface reflectance calibration of terrestrial imaging spectroscopy data: a tutorial using AVIRIS. In AVIRIS workshop proceedings [online]. Available: ftp://popo.jpl.nasa.gov/pub/docs/workshops/02_docs/2002_Clark_web.pdf [August 12, 2003].

DeBano, L. F.; Neary D.G.; Ffolliott, P.F. 1998. Fire effects on ecosystems. New York: John Wiley and Sons. 352 p.

DeBano L.F. 2000. The role of fire and soil heating on water repellency in wildland environments: a review. Journal of Hydrology. 231–232: 195–206.

Dekker L.W.; Ritsema C.J. 1994. How water moves in a water repellent sandy soil. Part 1: Potential and actual water repellency. Water Resources Research. 30: 2507–2517.

Elvidge, C.D. 1990. Visible and near infrared reflectance characteristics of dry plant materials. International Journal of Remote Sensing. 11(10): 1775 –1795.

Gao, B.C.; Heidebrecht, K.B.; Goetz, A.F.H. 1993. Derivation of scaled surface reflectances from AVIRIS data. Remote Sensing of Environment. 44: 165 –178.

Gao, B.C.; Heidebrecht, K.B.; Goetz A.F.H. 1999. Atmospheric removal program (ATREM) user's guide, version 3.1. Boulder, CO: Center for the Study of Earth from Space (CSES). 32 p.

Graham, R.T., ed. 2003. Hayman fire case study. Gen. Tech. Rep. RMRS-GTR-114 (revised). Ogden, UT: U.S. Department of Agriculture, Forest Service, Rocky Mountain Research Station. 404 p.

Jain, T.B. 2002. Burn-severity analysis data form. Unpublished study plan on file at U.S. Department of Agriculture, Forest Service, Rocky Mountain Research Station, Moscow, ID.

Key, C.H.; Benson, N.C. 2002. The normalized difference burn ratio (NDBR): a Landsat TM radiometric measure of burn severity [online]. Available: http://www.nrmsc.usgs.gov/research/ndbr.htm [August 12, 2004]

Letey, J.; Carillo, M.L.K.; Pang, X.P. 2000. Review: approaches to characterize the degree of water repellency. Journal of Hydrology. 231–232: 61–65.

Orlemann, A.; Saurer, M.; Parsons, A.; Jarvis, B. 2002. Rapid delivery of satellite imagery for burned area emergency response (BAER). In Proceedings of the ninth biennial Forest Service remote sensing applications conference, April 8–12, 2002, San Diego, CA. Bethesda, MD: American Society for Photogrammetry and Remote Sensing. Unpaginated CD-ROM.

Parsons, A. 2003. Burned area emergency rehabilitation (BAER) soil burn-severity definitions and mapping guidelines. Rep. No. RSAC-2999-RPT1. Salt Lake City, UT: U.S. Department of Agriculture, Forest Service, Remote Sensing Applications Center. 9 p.

Roberts, D.A.; Smith, M.O.; Adams, J.B. 1993. Green vegetation, nonphotosynthetic vegetation and soils in AVIRIS data. Remote Sensing of Environment. 44: 255 –269.

Rouse, J.W.; Haas, R.H.; Schell, J.A.; Deering, D.W. 1973. Monitoring vegetation systems in the Great Plains with ERTS. In Proceedings of the third earth resources technology satellite-1 symposium, NASA Goddard Space Flight Center, Greenbelt, MD. Washington, DC: NASA, SP-351: 309 –317.

Ryan, KC. 2002. Dynamic interactions between forest structure and fire behavior in boreal ecosystems. Silva Fennica. 36(1**)**: 13–39.

Ryan, K.C.; Noste, N.V. 1983. Evaluating prescribed fires. In Lotan, J.E.; Kilgore, B.M.; Fischer, W.C.; Mutch, R.W., eds. Proceedings of the symposium and workshop on wilderness fire. Gen. Tech. Rep. INT-182. Ogden, UT: U.S. Department of Agriculture, Forest Service, Intermountain Research Station: 230–238.